Journal of the Optical Society of America B
OPTICAL PHYSICS

Spin–orbit-coupling-induced broadband single-photon nonreciprocity on a solid-state platform

Yurou Chen,[1,2] Jiangnan Qin,[1] Binbin Zhang,[1] Yufei Wang,[1] Mingyuan Chen,[3] Shuangli Fan,[1,6] Mingwei Liu,[4,7] Xiao-Tao Xie,[1] Ren-Gang Wan,[1] Hongjun Zhang,[1] Keyu Xia,[3,5,8] and Hui Sun[1,*]

[1]School of Physics and Information Technology, Shaanxi Normal University, Xi'an 710062, China
[2]Avic Xi'an Aeronautics Computing Technique Research Institute, Xi'an 710005, China
[3]College of Engineering and Applied Sciences, National Laboratory of Solid State Microstructures, Collaborative Innovation Center of Advanced Microstructures, and School of Physics, Nanjing University, Nanjing 210093, China
[4]School of Physics and Electronic Science, Hunan University of Science and Technology, Xiangtan, Hunan 411201, China
[5]Jiangsu Key Laboratory of Artificial Functional Materials, and Key Laboratory of Intelligent Optical Sensing and Manipulation, Ministry of Education, Nanjing University, Nanjing 210093, China
[6]fanshuangli@snnu.edu.cn
[7]phymwliu@foxmail.com
[8]keyu.xia@nju.edu.cn
*physunh@snnu.edu.cn

Received 28 November 2024; revised 11 February 2025; accepted 16 February 2025; posted 18 February 2025; published 26 March 2025

Nonreciprocal optical devices (NRODs) working in the quantum regime are the key building blocks for nonreciprocal quantum information processing. Conventional NRODs require a bias field, such as a strong control field or an external magnetic field, increasing the complexity in fabrication and operation. Here, we propose a bias-free nonmagnetic scheme for single-photon isolators and circulators on a solid-state platform. Our single-photon isolator is made of a chiral optical waveguide embedded with a negatively charged carbon nanotube quantum dot (CNQD), while the circulator with four ports consists of two optical waveguides and a whispering-gallery-mode optical microresonator coupling to a CNQD in a chiral way. The time-reversal symmetry in these two systems breaks because the inherent spin–orbit coupling of electrons and holes in the CNQD strongly lifts the energy degeneracies of two circularly polarized transitions. Under realistic experimental parameters, we obtain a low-loss and high-isolation-contrast single-photon isolator over a 10 gigahertz bandwidth and a circulator over a one gigahertz bandwidth, respectively, without requiring any bias (control) fields. Our bias-free design can greatly simplify the implementation and operation of NRODs and provide a compact solid-state platform for nonreciprocal quantum information processing.

https://doi.org/10.1364/JOSAB.550334

1. INTRODUCTION

Nonreciprocal optical devices (NRODs) break the time-reversal symmetry (TRS) in optics and allow unidirectional propagation of light. Because of this nonreciprocity, NRODs, such as optical isolators and optical circulators, promise interesting applications in optical information processing [1–3]. NRODs working in the quantum regime can enhance photon-based quantum information processes [4–6] and are crucial elements for quantum networks [4]. The study in this direction has led to an emerging field of "chiral quantum optics" [6–34].

Faraday isolators and gyrators can break the TRS but are typically bulky [1]. When such magneto-optical devices are integrated on a chip, they become very lossy. Optical nonlinearity and photonic crystal heterojunctions can be used to realize optical isolators and circulators [34–41]. Furthermore, the breakdown of TRS has also been demonstrated in parity-time symmetry-broken systems [42–44] and spatio-temporal modulated waveguides [7,45,46], whereas these kinds of devices fail to isolate single photon. When applying these nonreciprocal devices to quantum applications, such as quantum simulation and quantum information processing [4], strong nonreciprocal (i.e., isolation contrast $\eta \to 1$ [8]), low loss, and compatibility with low light even to the single-photon level are crucial. Alternative strategies for breaking TRS have been pursued by exploiting chiral light–matter interaction [8–10],

a moving photonic crystal [13], moving cold atomic Bragg lattices [47], optomechanical systems [12,48,49], the Fizeau light-dragging effect in spinning optical resonator [23,24] and spinning yttrium iron garnet sphere [50,51], asymmetric cavity [52], directional quantum squeezing [53,54], and so on [33,55,56]. Recent theoretical [15] and experimental [18–21] progresses demonstrated that the TRS can also be broken by the random thermal motion of atoms, consequently resulting in a nonmagnetic optical isolator and circulator.

Nanophotonic waveguide with embedded quantum dot (QD) [57–66] is a promising solid-state platform for demonstrating spin-based quantum-optical components, such as optical isolators and circulators, due to their inherent scalability and mature semiconductor technology. In particular, photons in photonic crystal waveguides can be interfaced with QDs with near-unity efficiency [65]. In such a complex quantum architecture, the TRS can be broken by introducing a magnetic field [16,58,59] and controlling the spin of an electron or hole [59–61]. In QDs, the two-fold degeneracy can be lifted owing to the Zeeman shift, consequently resulting in the propagation-direction-dependent transmission. While the introduction of the external magnetic field could hamper the performance of nearby devices, one question is whether there exists a nonreciprocal structure that is made of a nanophotonic waveguide and QDs and can break TRS without the presence of a magnetic field for nonreciprocal integrated photonics.

In this manuscript, we suggest a bias-free nanophotonic waveguide–carbon nanotube quantum dot (CNQD) scheme for a bias-free single-photon isolator and circulator. In carbon nanotubes, due to the strong spin–orbit coupling (SOC), the zero-magnetic-field four-fold degenerate states split into two pairs of doublet states [67–72]. We show that the SOC-induced breakdown of electron–hole symmetry breaks the TRS, therefore supporting the bias-free broadband and low-loss single-photon isolators and circulators. The new physical approach for single-photon nonreciprocity naturally supports the achievement of optical isolators and circulators for bias-free spin-based solid-state quantum information processing on-chip.

2. SINGLE-PHOTON ISOLATOR

The schematic for realizing a bias-free single-photon isolator via a chiral scattering process is depicted in Fig. 1(a). A single negatively charged CNQD is embedded in a chiral photonic waveguide. In this nonreciprocal device, the light propagating along the photonic crystal waveguide is circularly polarized near holes and is subject to the spin–momentum locking [73–75]. The chiral waveguide can also be realized with an optical nanofiber or the interface of two photonic crystal structures supporting a chiral band edge mode. We assume that the single-polarized single-mode waveguide supports the circular polarization of photons at the position of CNQD. The circular polarization (chirality) of light depends upon the propagation direction. When the photon is right-moving with the wave vector $\vec{k}$ (left-moving with the opposite wave vector $-\vec{k}$), the polarization of the light at the location of CNQD is σ_+-circular (σ_--circular) polarized. Owing to the TRS, the right- and left-moving modes are related to each other via $\vec{E}_{\vec{k}} = \vec{E}^*_{-\vec{k}}$.

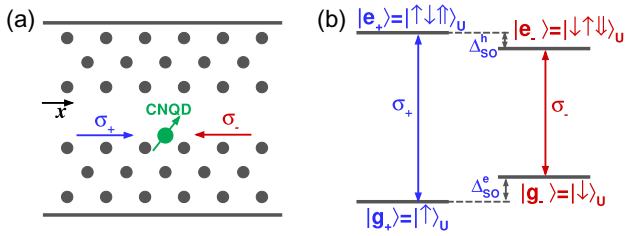

Fig. 1. Schematics of the single-photon isolator. (a) Chiral scattering of a single photon by a CNQD coupling to a photonic crystal waveguide. The right-moving and left-moving photons at the location of CNQD are denoted by σ_+ and σ_-, respectively. (b) Energy levels of a singly negatively charged CNQD in the trion picture only with positive orbital magnetic momentum (denoted by U). $\uparrow$ and $\downarrow$ ($\Uparrow$ and $\Downarrow$) denote the electron (heavy hole) with spin up and down. $|\uparrow\rangle$ and $|\downarrow\rangle$ ($|\Uparrow\rangle$ and $|\Downarrow\rangle$) denote the electron (heavy hole) spin states with $s^e_z = \hbar/2$ and $s^e_z = -\hbar/2$ ($s^h_z = 3\hbar/2$ and $s^h_z = -3\hbar/2$). Δ^e_{SO} and Δ^h_{SO} are the energy shifts of electron and heavy hole owing to the SOC.

According to the angular momentum conservation and Pauli's exclusion principle, when an electron is spin up $|\uparrow\rangle$ (spin down $|\downarrow\rangle$), a spin-down $|\downarrow\rangle$ (spin up $|\uparrow\rangle$) electron can be excited by the right-moving σ_+-polarized (left-moving σ_--polarized) photon from the valance band to conductive band, and therefore yielding a three-particle state $|\uparrow\downarrow\Uparrow\rangle$ ($|\downarrow\uparrow\Downarrow\rangle$). In carbon nanotubes, the electron possesses an orbital (valley) degree of freedom at Dirac points in the first Brillouin zone, leading to doubly degenerate electronic orbits. One electronic orbit circulates around the nanotube's circumference in a clockwise (CW) fashion, and the other circulates in the counterclockwise (CCW) direction. These two counter-propagating electron motions effectively generate microelectronic currents and give rise to "positively" (denoted by U) and "negatively" (denoted by D) oriented orbital magnetic moments. The coupling between the spin and orbital motion of electrons and holes leads to the splitting of the zero-field four-fold degeneracy into two pairs of doublet states with parallel and antiparallel spin and orbital magnetic moments [67,69], leading to the breakdown of the electron–hole transition degeneracy. Because of the momentum conservation, optical transitions are allowed only for U $\rightarrow$ U or D $\rightarrow$ D. In the trion picture, the energy level diagram of singly negatively charged CNQD associated with positive orbital magnetic momentum is depicted in Fig. 1(b). Δ^e_{SO} and Δ^h_{SO} represent the zero-field splitting of the electron and heavy hole between states with parallel and antiparallel spin and orbit magnetic moments. The subscript SO and superscripts e/h denote the SOC and electron/heavy hole, respectively. We prepare the electron in $|\uparrow\rangle_U$ state, and control the energy of the photons to be resonant with the $|\uparrow\rangle_U \leftrightarrow |\uparrow\downarrow\Uparrow\rangle_U$ transition. The transition $|\downarrow\rangle_U \leftrightarrow |\downarrow\uparrow\Downarrow\rangle_U$ is detuned by $\Delta_{SO} = \Delta^e_{SO} + \Delta^h_{SO}$ from the left-moving photons, and therefore, the CNQD is decoupled from the system. The transmission of the right-moving σ_+-polarized photon is different from that of the left-moving σ_--polarized photon. More importantly, the two circularly polarized photon-driven transitions inherently have nondegenerate energies without requiring any external bias fields. We will combine these bias-free chiral transitions of the CNQD and the spin–momentum locking to achieve a single-photon isolator and circulator. This is the basic idea of the present paper.

For the sake of simplicity, we denote $|\uparrow\rangle_U$ ($|\downarrow\rangle_U$) and $|\uparrow\downarrow\Uparrow\rangle_U$ ($|\downarrow\uparrow\Downarrow\rangle_U$) as $|g_+\rangle$ ($|g_-\rangle$) and $|e_+\rangle$ ($|e_-\rangle$), respectively. The subscript $\pm$ corresponds to the spin of CNQD. By linearizing the dispersion of the waveguide and applying the dipole and rotating-wave approximations, the Hamiltonian describing the interaction of the CNQD and the traveling single photon includes two contributions $H = H_0 + H_I$, where the free Hamiltonian H_0 and the interaction Hamiltonian H_I in real space are, respectively, given as ($\hbar = 1$) [76–78]:

$$H_0 = \int \mathrm{d}x \left[\hat{C}_R^\dagger \left(\omega_p - i v_g \frac{\partial}{\partial x}\right)\hat{C}_R + \hat{C}_L^\dagger \left(\omega_p + i v_g \frac{\partial}{\partial x}\right)\hat{C}_L\right] + (\omega_e - i\gamma)|e_+\rangle\langle e_+| + \omega_g|g_+\rangle\langle g_+| + (\omega_e - \Delta_{SO}^h - i\gamma)|e_-\rangle\langle e_-| + (\omega_g + \Delta_{SO}^e)|g_-\rangle\langle g_-|, \tag{1}$$

$$H_I = V\int \mathrm{d}x\delta(x)\left(|e_+\rangle\langle g_+|\hat{C}_R + |e_-\rangle\langle g_-|\hat{C}_L + \mathrm{h.c.}\right), \tag{2}$$

where $\hat{C}_R^\dagger$ and $\hat{C}_L^\dagger$ are Bosonic operators creating a right-moving and left-moving photon at x. The transition $|g_+\rangle \leftrightarrow |e_+\rangle$ is coupled by σ_+-polarized photons with V being the coupling strength. v_g denotes the group velocity of the photon in the waveguide. γ is the decay rate of the excited state $|e_+\rangle$. In Eq. (1), the first and second terms describe the free evolutions of the right- and left-moving modes, and the last four terms are the free Hamiltonian of the CNQD. The Hamiltonian H_I describes the interaction between the CNQD and the traveling modes.

The arbitrary general state $|\Psi(t)\rangle$ of the system can be expanded as

$$|\Psi(t)\rangle = [\int dx \left(\tilde{\phi}_R\hat{C}_R^\dagger + \tilde{\phi}_L\hat{C}_L^\dagger\right) + \tilde{e}_+|e_+\rangle\langle g_+| + \tilde{e}_-|e_-\rangle\langle g_-|]|0\rangle, \tag{3}$$

where $|0\rangle$ is the vacuum state with zero photons in the waveguide and with the CNQD in single-electron spin states. $\tilde{\phi}_R(\tilde{\phi}_L)$ is the wave function of the right-moving (left-moving) photons and $\tilde{e}_\pm$ being the excitation of the CNQD. The temporal evolution of $|\Psi(t)\rangle$ is described by the Schrödinger equation $i\partial_t|\Psi(t)\rangle = H|\Psi(t)\rangle$.

When the photon is input from the left-hand side, the Schrödinger equation gives

$$i\frac{\partial}{\partial t}\tilde{\phi}_R = \left(\omega_p - i v_g\frac{\partial}{\partial x}\right)\tilde{\phi}_R + V\delta(x)\tilde{e}_+, \tag{4}$$

$$i\frac{\partial}{\partial t}\tilde{e}_+ = V\delta(x)\tilde{\phi}_R + (\omega_e - i\gamma)\tilde{e}_+. \tag{5}$$

For the left-moving photon, the Schrödinger equation reads

$$i\frac{\partial}{\partial t}\tilde{\phi}_L = \left(\omega_p + i v_g\frac{\partial}{\partial x}\right)\tilde{\phi}_L + V\delta(x)\tilde{e}_-, \tag{6}$$

$$i\frac{\partial}{\partial t}\tilde{e}_- = V\delta(x)\tilde{\phi}_L + (\omega_e - \Delta_{SO} - i\gamma)\tilde{e}_-. \tag{7}$$

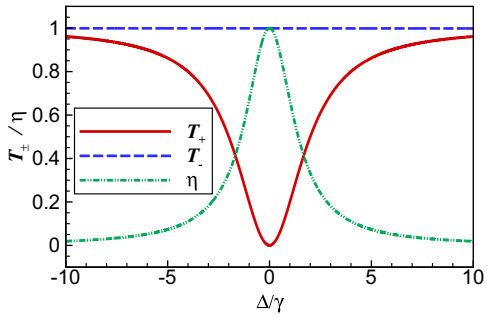

Fig. 2. Nonreciprocal transmissions T_+ (solid red curve), T_- (dashed blue curve), and isolation contrast η (long-dashed green curve) versus the detuning Δ. Γ is taken as $\Gamma = \gamma = 1$, and $\Delta_{SO} = 60\gamma$.

Following the standard processes of the photon transport method [77,78], the transmission amplitudes read

$$t_\pm = 1 + \frac{2i\Gamma}{\Delta_\pm - i(\gamma + \Gamma)}, \tag{8}$$

where $\Delta_+ = \omega - \omega_p = \Delta$, $\Delta_- = \omega - \omega_p - \Delta_{SO} = \Delta - \Delta_{SO}$, and $\Gamma = |V|^2/2v_g$ is the dissipation rate of CNQD due to the coupling to the waveguide. The first and second terms of $t_\pm$ describe the incoming photons emitting into the forward direction of the waveguide of the right-moving/left-moving photon due to the coherent scatter of the CNQD. For the right-moving photon, a Lorentz line shape absorption dip with width $2(\gamma + \Gamma)$ emerges due to the destructive interference. At $\Delta = 0$, $T_+ = 0$ could be achieved. Owing to SOC, the electron can be prepared in a spin-up state $|\uparrow\rangle_U$ by cooling. As a result, for the left-moving photons, the CNQD is decoupled. One immediately has $T_- = 1$. Transmissions are defined as $T_\pm = |t_\pm|^2$. The transmissions of T_+ (solid red curve) and T_- (dashed blue curve) with $\Gamma = \gamma = 1$ are shown in Fig. 2.

Throughout the following investigation, our discussion will be based on the experimentally measured values for the SOC in the CNQD [67,68]. We consider a CNT with diameter $d \sim 1.2$ nm and near-infrared lowest optical transition ($\sim$1.5 μm). We take $\gamma = 10.0$ GHz for the intrinsic decay rate of the CNQD [71], the corresponding exciton recombination time is about 100 ps. The energy differences induced by the SOC of the electron and heavy hole are, respectively, $\Delta_{SO}^e \simeq 374.06$ GHz ($\sim$1.55 meV) and $\Delta_{SO}^h \simeq 226.85$ GHz ($\sim$0.94 meV) [67], yielding $\Delta_{SO} = \Delta_{SO}^e + \Delta_{SO}^h \simeq 60\gamma$. Owing to the strong SOC, the $|\downarrow\rangle_U \leftrightarrow |\downarrow\uparrow\Downarrow\rangle_U$ transition is far detuned from the left-moving photons, and the electron could be prepared in a spin-up state $|\uparrow\rangle_U$ by cooling the CNQD below 17.4 K.

The isolation power of the isolator can be characterized by the absolute value of the isolation contrast, defined as $\eta = |T_- - T_+|/|T_- + T_+|$ [79], and the insertion loss, which is given by $-10\log(\mathrm{Max}\{T_+, T_-\})$. In Fig. 3, we show the isolation contrast η as a function of Δ and $\alpha = \Gamma/\gamma$. We can see that the SOC results in a nonreciprocal-transmission window where the single photon is on resonance with the corresponding transition of the CNQD. In the critical coupling regime, i.e., $\alpha = 1$, the single right-moving photon transition ideally equals zero at the CNQD transition frequency due to the destructive interference between the input and the coherent scattered parts of

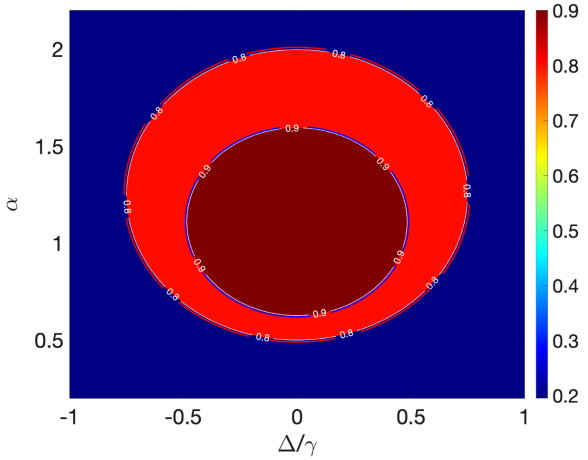

Fig. 3. Isolation contrast η as a function of Δ and α. γ and Δ_{SO} are taken as $\gamma = 10.0$ GHz and $\Delta_{SO} = 60\gamma$.

the photon. The right-moving single photon is σ_+-polarized at $x = 0$. At $\Delta = 0$, it critically couples to the CNQD and thus is blocked due to the destructive interference. In contrast, the left-moving photon is σ_--polarized at $x = 0$ and is off resonance with the corresponding transition of the CNQD. Furthermore, the electron spin-down state $|\downarrow\rangle_U$ is empty. As a result, the backward transmission is nearly unitary. Our single-photon isolator is broadband and robust against the variation of α. From Fig. 3, we can see the isolation contrast can be larger than 0.90 when $(\Delta/\gamma)^2 + (\alpha - 1.11)^2 \leq 0.49^2$, yielding a bandwidth of $\gamma_{\text{width}} \approx 10$ GHz. In this region, the corresponding insertion loss is less than 0.6 dB.

3. SINGLE-PHOTON CIRCULATOR

We consider a chiral quantum optical system shown in Fig. 4, which consists of two waveguides (bottom bus waveguide and top drop waveguide), a microresonator supporting chiral WGMs, and a singly negatively charged CNQD. The two waveguides have four ports P_i $(i = 1 - 4)$. The WGM microresonator is modeled as a single-mode resonator with frequency ω_c and two chiral modes, corresponding to a counter-clockwise (CCW)-propagating σ_+-polarized mode and a clockwise (CW)-propagating σ_--polarized one. The P_1- and P_3-input linearly polarized light excites the σ_+-polarized CCW mode, whereas the P_2 and P_4 inputs drive the σ_--polarized CW mode. κ_b (κ_d) is the coupling from the bottom bus (top drop) waveguide into the microresonator and vise versa. As shown in Fig. 1(b), the σ_+- and σ_--polarized modes drive the transitions $|\uparrow\rangle_U \leftrightarrow |\uparrow\downarrow\Uparrow\rangle_U$ and $|\downarrow\rangle_U \leftrightarrow |\downarrow\uparrow\Downarrow\rangle_U$, respectively. Due to the SOC, the frequencies of two chiral transitions of the CNQD differ by Δ_{SO}. At the same time, the electron is prepared in a spin-up state. Thus, only the transition $|\uparrow\rangle_U \leftrightarrow |\uparrow\downarrow\Uparrow\rangle_U$ resonantly couples to the corresponding WGM, while the other is completely decoupled from the resonator. This chiral interaction enables us to achieve a four-port circulator for single photons.

The transmissions into the bus and drop waveguides can be derived by the single-photon scattering method [8,78]. The transmission amplitudes t_{ij} indicate the scattering of single

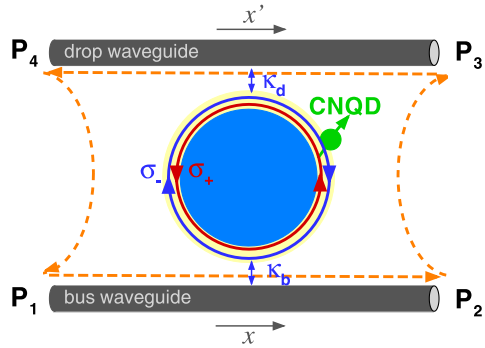

Fig. 4. Schematic proposed for a four-port bias-free single-photon circulator, consisting of two waveguides evanescently coupled to a WGM microresonator interacting with a CNQD. Two waveguides support four ports P_i $(i = 1 - 4)$. The microresonator supports two internal modes, i.e., a σ_+-polarized counter-clockwise mode and a σ_--polarized clockwise one. A negatively charged CNQD interacts with the σ_+ and σ_- modes. The interacting configuration is shown in Fig. 1(b). x and x' indicate the location in the bus and drop waveguides. T_{ij} $(i,\ j = 1 - 4$ and $i \neq j)$ denotes the transmission of a single photon from P_i to P_j.

photons from port P_i to port P_j $(i,\ j = 1 - 4$ and $i \neq j)$. They are evaluated as

$$t_{12/34} = 1 + \frac{2i\kappa_{b/d}}{\Delta_c - i\kappa - g^2/(\Delta_+ - i\gamma)}, \tag{9a}$$

$$t_{23} = t_{41} = \frac{2i\sqrt{\kappa_b\kappa_d}}{\Delta_c - i\kappa - g^2/(\Delta_- - i\gamma)}, \tag{9b}$$

$$t_{21/43} = 1 + \frac{2i\kappa_{b/d}}{\Delta_c - i\kappa - g^2/(\Delta_- - i\gamma)}, \tag{9c}$$

$$t_{14} = t_{32} = \frac{2i\sqrt{\kappa_b\kappa_d}}{\Delta_c - i\kappa - g^2/(\Delta_+ - i\gamma)}, \tag{9d}$$

where $\kappa_{b/d} = V_{b/d}^2/2v_g$ is the decay rates of the resonator due to the external coupling V_b (V_d) to the bus (drop) waveguide. Photons in both of the bus and drop waveguides are assumed to have the same group velocity v_g. $\kappa = \kappa_b + \kappa_d + \kappa_i$ denotes the total decay rate of the resonator with κ_i being the intrinsic decay rate. The two transitions of the CNQD have the same dipole moments. Thus, the coupling strength between the σ_+-polarized WGM and the transition $|\uparrow\rangle_U \leftrightarrow |\uparrow\downarrow\Uparrow\rangle_U$ equals to that between the σ_--polarized mode and the transition $|\downarrow\rangle_U \leftrightarrow |\downarrow\uparrow\Downarrow\rangle_U$, denoted as g. The detuning Δ_c is defined as $\Delta_c = \omega_c - \omega_p$ with ω_p being the frequency of the single-photon input. The transmissions are given by $T_{ij} = |t_{ij}|^2$.

Here is the basic idea for the single-photon circulator. To focus on the idea, we consider $\kappa_b = \kappa_d \gg \kappa_i$ and $\omega_c = \omega_p$. We take $\Delta_+ \to 0$ and $|\Delta_{SO}| \gg g$ for instance. A single-photon input to port 1 or 3 drives the σ_+-polarized WGM mode, which is resonant with the $|\uparrow\rangle_U \leftrightarrow |\uparrow\downarrow\Uparrow\rangle_U$ transition of the CNQD. This strong resonator–CNQD coupling suppresses the resonator excitation and subsequently leads to the maximal transmission in the waveguide:

$$T_{12} = T_{34} \simeq \frac{(\kappa_i\gamma + g^2)^2 + \Delta^2(\kappa_i + \gamma)^2}{(\kappa\gamma + g^2)^2 + \Delta^2(\kappa + \gamma)^2}. \tag{10}$$

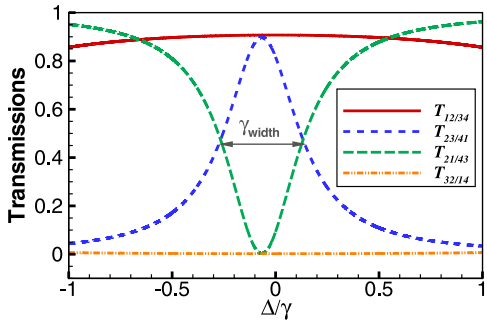

Fig. 5. T_{ij} $(i,\ j=1-4$ and $i\neq j)$ as functions of detuning Δ with $g=2\gamma$, $\kappa_{\rm b}=\kappa_{\rm d}=10^{-1}\gamma$, and $\kappa_{\rm i}=10^{-2}\gamma$. Other parameters are taken as those in Fig. 3.

A single photon entering the system through port 2 or 4 excites the σ_--polarized WGM mode and excites the transition $|\downarrow\rangle_{\rm U}\leftrightarrow|\downarrow\uparrow\Downarrow\rangle_{\rm U}$. T_{23} and T_{41} exhibit Lorentz shaped [see Eq. (9b)] around $\Delta=-[g^2/(\Delta_{\rm SO}^2+\gamma^2)]\Delta_{\rm SO}$, and the full width at half-maxima (FWHM) read

$$\gamma_{\rm width}=2\kappa\left[1+\left(\frac{g^2}{\kappa\gamma}\right)\left(\frac{\gamma^2}{\Delta_{\rm SO}^2}\right)\right]. \tag{11}$$

At $\Delta=\Delta_{\rm max}=-[g^2/(\Delta_{\rm SO}^2+\gamma^2)]\Delta_{\rm SO}$, the cross transmissions T_{23} and T_{41} reach their maximum values, about $(4\kappa_{\rm b}\kappa_{\rm d}/\kappa^2)[1+(g^2/\kappa\gamma)(\gamma^2/\Delta_{\rm SO}^2)]^{-1}$. In the strong coupling regime $(\kappa\gamma\ll g^2)$, owing to the strong SOC $(\Delta_{\rm SO}\simeq 60\gamma$ in the present CNQD), we have $\Delta_{\rm max}\to 0$ and thus $T_{12}=T_{34}=T_{23}=T_{41}\sim 1$ with $\kappa\gg\kappa_i$ at $\Delta=\Delta_{\rm max}$. At the same time, under these conditions, the crossing transmissions $T_{14/32}$ and $T_{21/43}$ are minimal, equal to $T_{14}=T_{32}\simeq 4\kappa_{\rm b}\kappa_{\rm d}\gamma^2/(\kappa\gamma+g^2)^2\to 0$ and $T_{21}=T_{43}\simeq(\kappa_i/\kappa)^2\to 0$, respectively. Thus, we obtain a good circulator with photons flowing along the CCW direction $({\rm P}_1\to{\rm P}_2\to{\rm P}_3\to{\rm P}_4\to{\rm P}_1)$.

The transmissions of T_{ij} $(i,\ j=1-4$ and $i\neq j)$ as functions of detuning Δ are shown in Fig. 5. The coupling strength g and decay rates are taken as $g=2\gamma$, $\kappa_{\rm b}=\kappa_{\rm d}=10^{-1}\gamma$, and $\kappa_{\rm i}=10^{-2}\gamma$. All other parameters are same as those in Fig. 3. Under this set of parameter conditions, one has $T_{12}=T_{34}$ [see Eq. (9a) and the solid red curve] and $T_{21}=T_{43}$ [see Eq. (9c) and the long-dashed green curve]. The transmissions T_{23} and T_{41} exhibit Lorentz shape with $\gamma_{\rm width}\simeq 0.422\gamma$ (see the dashed blue curve) and reach their maximum values 0.898 at $\Delta\simeq-0.066\gamma$. T_{21} and T_{43} are the inverted Lorentz line shape (see the green long-dashed curve). At the same parameter conditions, $T_{12}=T_{34}\simeq 0.907$, while $T_{21}=T_{43}\simeq 0.003$ and $T_{32}=T_{14}\simeq 0.002$. These numerical calculations show that the present WGM microresonator-CNQD quantum system supports CCW direction single-photon circulator with four ports.

The behavior of the circulator can be fully characterized by the fidelity $\mathcal{F}$ and the insertion loss $\mathcal{I}$ of the single-photon circulator with the transmission matrix $\tilde{T}$. The fidelity $\mathcal{F}$ gives the probability of a correct circulator operation averaged over all input cases, and it is defined as $\mathcal{F}={\rm Tr}[\tilde{T}T^{{\rm id},T}]/{\rm Tr}[T^{\rm id}T^{{\rm id},T}]$ [9,15] with $\tilde{T}=\{T_{ij}/\eta_i\}$ being the renormalized transmission matrix and $T^{\rm id}$ the ideal one of a four-port circulator [9,15]. $\eta_i=\sum_k T_{ik}$ describes the survival probability of the probe photons entering waveguides rather than loss [9,15,21]. The average photon survival probability is given by $\eta=\sum_{i=1}^4\eta_i/4$. The insertion loss is given by $\mathcal{I}=-10\log_{10}(\eta)$.

The fidelity $\mathcal{F}$ and insertion loss $\mathcal{I}$ are depicted as functions of Δ and g, respectively, in Fig. 6. The decay rates $\kappa_{\rm b/d}$ for calculations are $\kappa_{\rm b}=\kappa_{\rm d}=10^{-1}\gamma$ and $\kappa_{\rm i}=10^{-2}\gamma$. γ and $\Delta_{\rm SO}$ are same as those in Fig. 3. Around $\Delta\approx 0$, large fidelity $(\mathcal{F}\geq 0.8)$ associated with low insertion loss $(\mathcal{I}\leq 1.5$ dB) can be achieved when $g\geq 0.5$. When $g=2\gamma$, the fidelity approaches unity, ≈ 0.99 at $\Delta=\Delta_{\rm max}\approx-0.66$ GHz. Meanwhile, the insertion loss is small, about 0.4 dB [see Fig. 6(b)]. The isolations, which are defined as $I_i=10\log(T_{ij}/T_{ji})$ [9], of the four-port circulator formed between adjacent ports are $\{I_i\}=\{25.14,25.97,25.14,25.97\}$ dB, implying the nonreciprocal photon circulating along the CCW direction. Due to the giant dipole moment of CNQDs [80–82], the photon–CNQD coupling is large. This strong coupling creates a broadband nonreciprocal window of $|\Delta-\Delta_{\rm max}|<0.65$ GHz, where the fidelity is no less than 0.95 and the insertion loss is small, about 0.4 dB. Thus, using a CNQD coupling to a WGM microresonator, we can achieve a single-photon circulator with broad bandwidth (∼1.3 GHz), low insertion loss (≈0.4 dB), and high fidelity (>0.95).

4. CONCLUSION

In a solid-state picture, we propose a nanophotonic waveguide embedded with CNQD and a WGM microresonator coupled with CNQD for a bias-free nonmagnetic single-photon isolator and circulator with broad bandwidth, low insertion loss, and high fidelity simultaneously. Our study demonstrates, in these

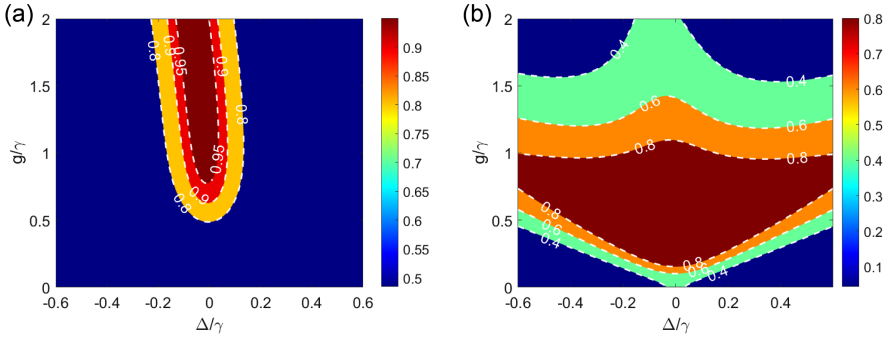

Fig. 6. (a) Fidelity $\mathcal{F}$ and (b) insertion loss $\mathcal{I}$ of the single-photon circulator as functions of the detuning Δ and the resonator–CNQD coupling g. Other parameters for calculation are same as those in Fig. 5.

two hybrid quantum schemes, that the zero-magnetic-field spin splits of electron and heavy hole break the TRS, resulting in the nonreciprocal behaviors of single photons. Simultaneously, the nonreciprocal behaviors make the broadband (exceeding 1.3 GHz), low insertion loss (less than 0.6 dB), and high-fidelity (larger than 0.95) single-photon isolator and four-port single-photon circulator achievable. Remarkably, the nonreciprocal solid-state optical device without external bias and magnetic field is promising for miniaturization and integration on a chip. We believe our study paves the way for high-performance, bias-free, nonmagnetic, nonreciprocal optical devices for spin-based, solid-state, on-chip quantum information processing.

Funding. National Key Research and Development Program of China (2019YFA0308700, 2017YFA0303703, 2017YFA0303701); National Natural Science Foundation of China (11874212, 11890704, 61671279, 11574145, 11690031); Fundamental Research Funds for the Central Universities (021314380095); Xi'an Science and Technology Plan Project (23KGDW0026-2022).

Disclosures. The authors declare no conflicts of interest.

Data availability. Data underlying the results presented in this paper are not publicly available at this time but may be obtained from the authors upon reasonable request.

REFERENCES

1. D. Jalas, A. Petrov, M. Eich, *et al.*, "What is—and what is not—an optical isolator," Nat. Photonics **7**, 579–582 (2013).
2. Y. Shi, Z. Yu, and S. Fan, "Limitations of nonlinear optical isolators due to dynamic reciprocity," Nat. Photonics **9**, 388–392 (2015).
3. K. Y. Yang, J. Skarda, M. Cotrufo, *et al.*, "Inverse-designed non-reciprocal pulse router for chip-based LiDAR," Nat. Photonics **14**, 369–374 (2020).
4. H. J. Kimble, "The quantum internet," Nature **453**, 1023–1030 (2008).
5. L. Zhou, L.-P. Yang, Y. Li, *et al.*, "Quantum routing of single photonics with a cyclic three-level system," Phys. Rev. Lett. **111**, 103604 (2013).
6. P. Lodahl, S. Mahmoodian, S. Stobbe, *et al.*, "Chiral quantum optics," Nature **541**, 473–480 (2017).
7. D. L. Sounas and A. Alù, "Non-reciprocal photonics based on time modulation," Nat. Photonics **11**, 774–783 (2017).
8. K. Xia, G. Lu, G. Lin, *et al.*, "Reversible nonmagnetic single-photonics isolation using unbalanced quantum coupling," Phys. Rev. A **90**, 043802 (2014).
9. M. Scheucher, A. Hilico, E. Will, *et al.*, "Quantum optical circulator controlled by a single chirally coupled atom," Science **354**, 1577 (2016).
10. C. Sayrin, C. Junge, R. Mitsch, *et al.*, "Nanophotonics optical isolator controlled by the internal state of cold atoms," Phys. Rev. X **5**, 041036 (2015).
11. S.-H. Gong, F. Alpeggiani, B. Sciacca, *et al.*, "Nanoscale chiral valley-photonics interface through optical spin-orbit coupling," Science **359**, 443–447 (2018).
12. X. Xu, Y. Zhao, H. Wang, *et al.*, "Quantum nonreciprocality in quadratic optomechanics," Photonics Research **8**, 143–150 (2020).
13. D.-W. Wang, H.-T. Zhou, M.-J. Guo, *et al.*, "Optical diode made from a moving photonics crystal," Phys. Rev. Lett. **110**, 093901 (2013).
14. B. He, L. Yang, X. Jiang, *et al.*, "Transmission nonreciprocity in a mutually coupled circulating structure," Phys. Rev. Lett. **120**, 203904 (2018).
15. K. Xia, F. Nori, and M. Xiao, "Cavity-free optical isolators and circulators using a chiral cross-Kerr nonlinearity," Phys. Rev. Lett. **121**, 203602 (2018).
16. L. Tang, J. Tang, W. Zhang, *et al.*, "On-chip chiral single-photonics interface: isolation and unidirectional emission," Phys. Rev. A **99**, 043833 (2019).
17. T. Li, A. Miranowicz, X. Hu, *et al.*, "Quantum memory and gates using a Λ-type quantum emitter coupled to a chiral waveguide," Phys. Rev. A **97**, 062318 (2018).
18. S. Zhang, Y. Hu, G. Lin, *et al.*, "Thermal-motion-induced non-reciprocal quantum optical system," Nat. Photonics **12**, 744–748 (2018).
19. G. Lin, S. Zhang, Y. Hu, *et al.*, "Nonreciprocal amplification with four-level hot atoms," Phys. Rev. Lett. **123**, 033902 (2019).
20. C. Liang, B. Liu, A.-N. Xu, *et al.*, "Collision-induced broadband optical nonreciprocity," Phys. Rev. Lett. **125**, 123901 (2020).
21. S. Zhang, G. Lin, Y. Hu, *et al.*, "Cavity-free circulator with low insertion loss using hot atoms," Phys. Rev. Appl. **14**, 024032 (2020).
22. W. Gou, T. Chen, D. Xie, *et al.*, "Tunable nonreciprocal quantum transport through a dissipative Aharonov-Bohm ring in ultracold atoms," Phys. Rev. Lett. **124**, 070402 (2020).
23. R. Huang, A. Miranowicz, J.-Q. Liao, *et al.*, "Nonreciprocal photonics blockade," Phys. Rev. Lett. **121**, 153601 (2018).
24. B. Li, R. Huang, X. Xu, *et al.*, "Nonreciprocal unconventional photonics blockade in a spinning optomechanical system," Photonics Res. **7**, 630–641 (2019).
25. Z. Wang, L. Du, Y. Li, *et al.*, "Phase-controlled single-photonics nonreciprocal transmission in a one-dimensional waveguide," Phys. Rev. A **100**, 053809 (2019).
26. K. Wang, Q. Wu, Y.-F. Yu, *et al.*, "Nonreciprocal photonics blockade in a two-mode cavity with a second-order nonlinearity," Phys. Rev. A **100**, 053832 (2019).
27. Y. Jiang, S. Maayani, T. Carmon, *et al.*, "Nonreciprocal phonon laser," Phys. Rev. Appl. **10**, 064037 (2018).
28. L. Du, Y.-T. Chen, J.-H. Wu, *et al.*, "Nonreciprocal interference and coherent photonics routing in a three-port optomechanical system," Opt. Express **28**, 3647–3659 (2020).
29. H. Z. Shen, Q. Wang, J. Wang, *et al.*, "Nonreciprocal unconventional photonics blockade in a driven dissipative cavity with parametric amplification," Phys. Rev. A **101**, 013826 (2020).
30. J.-S. Tang, W. Nie, L. Tang, *et al.*, "Nonreciprocal single-photonics band structure," Phys. Rev. Lett. **128**, 203602 (2022).
31. G.-L. Zhu, C.-S. Hu, H. Wang, *et al.*, "Nonreciprocal superradiant phase transitions and multicriticality in a cavity QED system," Phys. Rev. Lett. **132**, 193602 (2024).
32. A. Tripathi, C. F. Ugwu, V. S. Asadchy, *et al.*, "Nanoscale optical nonreciprocity with nonlinear metasurfaces," Nat. Commun. **15**, 5077 (2024).
33. S. Yang, M. Liu, C. Zhao, *et al.*, "Nonreciprocal thermal photonics," Nat. Photonics **18**, 412–424 (2024).
34. C. Kong, H. Xiong, and Y. Wu, "Magnon-induced nonreciprocity based on the magnon Kerr effect," Phys. Rev. Appl. **12**, 034001 (2019).
35. L. Fan, J. Wang, L. T. Varghese, *et al.*, "An all-silicon passive optical diode," Science **335**, 447–450 (2012).
36. Z. Shen, Y.-L. Zhang, Y. Chen, *et al.*, "Experimental realization of optomechanically induced non-reciprocity," Nat. Photonics **10**, 657–661 (2016).
37. Q.-T. Cao, H. Wang, C.-H. Dong, *et al.*, "Experimental demonstration of spontaneous chirality in a nonlinear microresonator," Phys. Rev. Lett. **118**, 033901 (2017).
38. N. Bender, S. Factor, J. D. Bodyfelt, *et al.*, "Observation of asymmetric transport in structures with active nonlinearities," Phys. Rev. Lett. **110**, 234101 (2013).
39. S. Hua, J. Wen, X. Jiang, *et al.*, "Demonstration of a chip-based optical isolator with parametric amplification," Nat. Commun. **7**, 13657 (2016).
40. K. Abdelsalam, T. Li, J. B. Khurgin, *et al.*, "Linear isolators using wavelength conversion," Optica **7**, 209–213 (2020).
41. A. D. White, G. H. Ahn, K. V. Gasse, *et al.*, "Integrated passive nonlinear optical isolators," Nat. Photonics **17**, 143–149 (2023).
42. B. Peng, S. K. Özdemir, F. Lei, *et al.*, "Parity–time-symmetric whispering-gallery microcavities," Nat. Phys. **10**, 394–398 (2014).
43. L. Chang, X. Jiang, S. Hua, *et al.*, "Parity–time symmetry and variable optical isolation in active–passive-coupled microresonators," Nat. Photonics **8**, 524–529 (2014).

44. J. Ma, J. Wen, S. Ding, *et al.*, "Chip-based optical isolator and nonreciprocal parity-time symmetry induced by stimulated Brillouin scattering," Laser Photonics Rev. **14**, 1900278 (2020).
45. Z. Yu and S. Fan, "Complete optical isolation created by indirect interband photonics transitions," Nat. Photonics **3**, 91–94 (2009).
46. A. E. Cardin, S. R. Silva, S. R. Vardeny, *et al.*, "Surface-wave-assisted nonreciprocity in spatio-temporally modulated metasurfaces," Nat. Commun. **11**, 1469 (2020).
47. S. A. R. Horsley, J.-H. Wu, M. Artoni, *et al.*, "Optical nonreciprocity of cold atom Bragg mirrors in motion," Phys. Rev. Lett. **110**, 223602 (2013).
48. M. Hafezi and P. Rabl, "Optomechanically induced non-reciprocity in microring resonators," Opt. Express **20**, 7672–7684 (2012).
49. X.-W. Xu and Y. Li, "Optical nonreciprocity and optomechanical circulator in three-mode optomechanical systems," Phys. Rev. A **91**, 053854 (2015).
50. X. Deng, K.-K. Zhang, T. Shui, *et al.*, "Nonreciprocal unconventional magnon blockade via the Sagnac-Fizeau shift in an optomagnonic system," Phys. Rev. A **110**, 063711 (2024).
51. X. Deng, K.-K. Zhang, T. Zhang, *et al.*, "Nonreciprocal unconventional photonics blockade via Barnett effect in a hybrid cavity magnonic system," Chaos Solitons Fractals **191**, 115880 (2025).
52. P. Yang, X. Xia, H. He, *et al.*, "Realization of nonlinear optical nonreciprocity on a few-photonics level based on atoms strongly coupled to an asymmetric cavity," Phys. Rev. Lett. **123**, 233604 (2019).
53. L. Tang, J. Tang, M. Chen, *et al.*, "Quantum squeezing induced optical nonreciprocity," Phys. Rev. Lett. **128**, 083604 (2022).
54. Y.-R. Zhou, Q.-F. Zhang, F.-F. Liu, *et al.*, "Controllable nonreciprocal phonon laser in a hybrid photonics molecule based on directional quantum squeezing," Opt. Express **32**, 2786–2803 (2024).
55. C. W. Peterson, W. A. Benalcazar, M. Lin, *et al.*, "Strong nonreciprocity in modulated resonator chains through synthetic electric and magnetic fields," Phys. Rev. Lett. **123**, 063901 (2019).
56. S. R.-K. Rodriguez and S. A. Mann, "Heat-assisted nonreciprocity," Nat. Photonics **18**, 5–6 (2024).
57. A. Javadi, I. Söllner, M. Arcari, *et al.*, "Single-photonics non-linear optics with a quantum dot in a waveguide," Nat. Commun. **6**, 8655 (2015).
58. E. J. Lenferink, G. Wei, and N. P. Stern, "Coherent optical nonreciprocity in axisymmetric resonators," Opt. Express **22**, 16099–16111 (2014).
59. A. Javadi, D. Ding, M. H. Appel, *et al.*, "Spin–photonics interface and spin-controlled photonics switching in a nanobeam waveguide," Nat. Nanotechnol. **13**, 398–403 (2018).
60. R. J. Coles, D. M. Price, J. E. Dixon, *et al.*, "Chirality of nanophotonics waveguide with embedded quantum emitter for unidirectional spin transfer," Nat. Commun. **7**, 11183 (2016).
61. C. Y. Hu, "Spin-based single-photonics transistor, dynamic random access memory, diodes, and routers in semiconductors," Phys. Rev. B **94**, 245307 (2016).
62. D. L. Hurst, D. M. Price, C. Bentham, *et al.*, "Nonreciprocal transmission and reflection of a chirally coupled quantum dot," Nano Lett. **18**, 5475–5481 (2018).
63. D. Hallett, A. P. Foster, D. L. Hurst, *et al.*, "Electrical control of nonlinear quantum optics in a nano-photonics waveguide," Optica **5**, 644–650 (2018).
64. J. Perczel, J. Borregaard, D. E. Chang, *et al.*, "Topological quantum optics using atomlike emitter arrays coupled to photonics crystals," Phys. Rev. Lett. **124**, 083603 (2020).
65. M. Arcari, I. Söllner, A. Javadi, *et al.*, "Near-unity coupling efficiency of a quantum emitter to a photonics crystal waveguide," Phys. Rev. Lett. **113**, 093603 (2014).
66. N. O. Antoniadis, N. Tomm, T. Jakubczyk, *et al.*, "A chiral one-dimensional atom using a quantum dot in an open microcavity," npj Quantum Inf. **8**, 27 (2022).
67. F. Kuemmeth, S. Ilani, D. C. Ralph, *et al.*, "Coupling of spin and orbital motion of electrons in carbon nanotubes," Nature **452**, 448–452 (2008).
68. G. A. Steele, F. Pei, E. A. Laird, *et al.*, "Large spin-orbit coupling in carbon nanotubes," Nat. Commun. **4**, 1573 (2013).
69. S. Weiss, E. I. Rashba, F. Kuemmeth, *et al.*, "Spin-orbit effects in carbon-nanotube double quantum dots," Phys. Rev. B **82**, 165427 (2010).
70. F. Kuemmeth, H. Churchill, P. Herring, *et al.*, "Carbon nanotubes for coherent spintronics," Mater. Today **13**(3), 18–26 (2010).
71. C. Galland and A. Imamoğlu, "All-optical manipulation of electron spins in carbon-nanotube quantum dots," Phys. Rev. Lett. **101**, 157404 (2008).
72. H. Sun, X.-L. Feng, S. Gong, *et al.*, "Giant cross-Kerr nonlinearity in carbon nanotube quantum dots with spin-orbit coupling," Phys. Rev. B **79**, 193404 (2009).
73. Z.-Q. Yang, Z.-K. Shao, H.-Z. Chen, *et al.*, "Spin-momentum-locked edge mode for topological vortex lasing," Phys. Rev. Lett. **125**, 013903 (2020).
74. I. Söllner, S. Mahmoodian, S. L. Hansen, *et al.*, "Deterministic photonics–emitter coupling in chiral photonics circuits," Nat. Nanotechnol. **10**, 775–778 (2015).
75. M. J. Mehrabad, A. P. Foster, R. Dost, *et al.*, "Chiral topological photonics with an embedded quantum emitter," Optica **7**, 1690–1696 (2020).
76. J.-T. Shen and S. Fan, "Strongly correlated two-photonics transport in a one-dimensional waveguide coupled to a two-level system," Phys. Rev. Lett. **98**, 153003 (2007).
77. J. T. Shen and S. Fan, "Coherent photonics transport from spontaneous emission in one-dimensional waveguides," Opt. Lett. **30**, 2001–2003 (2005).
78. J.-T. Shen and S. Fan, "Theory of single-photonics transport in a single-mode waveguide. I. Coupling to a cavity containing a two-level atom," Phys. Rev. A **79**, 023837 (2009).
79. Y. Shen, M. Bradford, and J.-T. Shen, "Single-photonics diode by exploiting the photonics polarization in a waveguide," Phys. Rev. Lett. **107**, 173902 (2011).
80. A. Graf, L. Tropf, Y. Zakharko, *et al.*, "Near-infrared exciton-polaritons in strongly coupled single-walled carbon nanotube microcavities," Nat. Commun. **7**, 13078 (2016).
81. W. Gao, X. Li, M. Bamba, *et al.*, "Continuous transition between weak and ultrastrong coupling through exceptional points in carbon nanotube microcavity exciton–polaritons," Nat. Photonics **12**, 362–367 (2018).
82. V. A. Shahnazaryan, V. A. Saroka, I. A. Shelykh, *et al.*, "Strong light–matter coupling in carbon nanotubes as a route to exciton brightening," ACS Photonics **6**, 904–914 (2019).